EUROPEAN ORGANIZATION FOR NUCLEAR RESEARCH

ANTIPROTON-PROTON ELASTIC SCATTERING AT 6.2 GeV/c

T. Buran[1], A. Eide[2,3], P. Helgaker[1], P. Lehmann, A. Lundby,
A. Navarro-Savoy, L. Staurset[1] and O. Sørum[1]
CERN, Geneva, Switzerland

C. Baglin, P. Briandet, P. Fleury, G. de Rosny and J.M. Thenard
Ecole Polytechnique, Paris, France

P.J. Carlson and K.E. Johansson
University of Stockholm, Sweden

B. d'Almagne, F. Richard and D. Treille
Laboratoire de l'Accélérateur Linéaire, Orsay, France

V. Gracco
University of Genoa and INFN, Genoa, Italy

ABSTRACT

Antiproton-proton elastic scattering data at 6.2 GeV/c in the range $0.3\ (\mathrm{GeV/c})^2 \leq -t \leq 10.0\ (\mathrm{GeV/c})^2$ is presented. The experiment, using spark chambers and proportional chambers, was performed at the CERN Proton Synchrotron.

The dip at about $-t = 0.5$ and the structure at about $-t = 2.2\ (\mathrm{GeV/c})^2$ are equally strong at 6.2 GeV/c as they are at 5.0 GeV/c. The differential cross-sections around 90° c.m. are not very different at 5.0 GeV/c and at 6.2 GeV/c, whereas in the backward region there is a decrease of the order of one magnitude.

Geneva - 23 June 1975
(Submitted to Nuclear Physics)

---

1) Present address: Department of Physics, University of Oslo, Oslo 3, Norway.

2) Present address: Agder Regional College, Box 607, N-4601 Kristiansand, Norway.

3) Supported in part by Ecole Polytechnique, Paris, France.

1. INTRODUCTION

In a series of experiments performed at the CERN PS, where we measured large-angle elastic scattering, we have earlier[1] reported results of $\pi^{\pm}p$, $K^{\pm}p$, and $\bar{p}p$ elastic scattering at 5 GeV/c incident momentum, and similarly $\pi^{+}p$ [2,3] and $K^{+}p$ [3,4] wide-angle elastic scattering at 10 GeV/c.

In this report we present results of $\bar{p}p$ elastic scattering at 6.2 GeV/c, in the interval $0.3 \leq -t \leq 10.0$ $(GeV/c)^2$. In the same experiment we have also results on $K^-p \to K^-p$, $\pi^-p \to \pi^-p$, $\bar{p}p \to \pi^-\pi^+$, and $\bar{p}p \to K^-K^+$ which will be published elsewhere.

The $\bar{p}p$ elastic scattering has been studied in the forward direction up to 100 GeV/c [5-12]. The dip at $-t = 0.5$ $(GeV/c)^2$ has been well studied particularly at rather low energies[5-9]. With increasing energy this dip seems to become less pronounced and moves towards larger absolute values of t.

Large-angle scattering data are less abundant. We have earlier presented an almost complete t-distribution of $\bar{p}p$ elastic scattering at 5 GeV/c. The most salient features are the very low cross-sections at large scattering angles, the lowest value being about 10 nb/$(GeV/c)^2$. We also observed a significant backward peak. The very rapid decrease in cross-section with increasing energy (s^{-10}) makes a detailed study of this angular region rather difficult at very much higher energies.

In Section 2 of this paper we discuss the apparatus, in Section 3 the data analysis, and in Section 4 we present the experimental results.

2. APPARATUS

This experiment was performed with an incident momentum of 6.2 GeV/c, in the same beam and with almost the same experimental equipment as for the positive 10 GeV/c experiment[2-4]. Hence we will only give a brief outline of the apparatus, and refer to other publications for further details[1-4].

2.1 Layout of experiment

The experimental layout is shown in Fig. 1. There are two liquid-hydrogen targets in the beam. This makes it possible to measure both small- and large-angle events in the same experiment, and it is always possible to determine the momentum of one of the two secondary particles.

The direction of the incident particles was measured by means of hodoscopes consisting of scintillation counters and proportional chambers. The direction of one of the outgoing particles was measured by wire spark chamber telescope W_1 if the incident particle reacted in target 1, and by telescope W_4 if the incident particle reacted in target 2. The other secondary particle was measured by W_3 after deflection in the magnetic field. A threshold Čerenkov counter CW_3 was

placed behind W_3. It was filled with freon at atmospheric pressure. During the analysis it was used to reduce the background from the sample of backward elastic scattered $\bar{p}p$ events.

2.2 Incident beam

The unseparated beam was produced at an internal target at the CERN Proton Synchrotron, and was the same as that used for the 10 GeV/c run[2-4]. The internal proton momentum was 19 GeV/c. With a momentum spread of ±1% the intensity of the secondary beam was approximately 5×10^5 particles per machine pulse, with an effective length of 350 msec and with a repetition time of 2 sec. The production angle was 40 mrad. The beam contained 1.1% antiprotons, 1.4% kaons, 94.5% pions, and 3% muons.

2.3 Spark chambers

The telescopes W_1, W_3, and W_4 in Fig. 1 contained wire chambers with core read-out. The two upstream chambers in W_2 also had core read-out, whereas the other four near or inside the magnet had capacity read-out. Wire spacing was 1 mm and the gap width was 1 cm. The construction and the performance of the wire chambers have been described elsewhere[1]. Typical cluster size was 3-6 wires. Roughly 1% of the clusters were split in two halves with more than one wire missing between them.

2.4 Spectrometer magnet

The C-frame-type magnet had a gap of $100 \times 100 \times 50$ cm^3 and with an integral $\int B \cdot d\ell$ of approximately 1.5 Tm.

The field components were measured at 37,800 points to an accuracy of 0.3% of the main component. During the experiment the stability of the magnetic field was monitored to an accuracy of better than 0.2%.

2.5 Trigger and counter logic

The incident beam was defined by the four scintillation counters S_1, S_2, S_3, S_4, and the three threshold gas Čerenkov counters C_1, C_2, and C_3. The counter V_1 vetoed the beam halo, while V_2 vetoed particles passing through both targets without interacting.

Trigger counters T_1, T_3, and T_4 were placed behind the corresponding spark chamber telescopes W_1, W_3, and W_4. The trigger counters consisted of two parallel arrays of scintillation counters, one having narrow vertical elements, whereas the other had wider horizontal elements.

The trigger counter T_1 or T_4 was used to decide if a beam particle defined by the coincidence $S_1 \cdot S_2 \cdot S_3 \cdot S_4 \cdot \bar{V}_1 \cdot \bar{V}_2$ *) had an interaction in target 1 or in target 2, respectively.

The signatures for the different particles were

$$\pi\colon\ (C_1 + C_3) \cdot C_2$$

$$K\colon\ C_1 \cdot \bar{C}_2 \cdot C_3$$

$$\bar{p}\colon\ \bar{C}_1 \cdot \bar{C}_2 \cdot \bar{C}_3$$

To get a restrictive trigger, only one signal was allowed in each of the arrays T_1, T_3, and T_4. Furthermore, a rough test on coplanarity was obtained by requiring that if one of the scattered particles hit the lower half of T_3, the other particle should hit the upper half of T_1 or T_4, and vice versa.

In addition to the "up-down" selection at the T_3 array, a "left-right" selection possibility was also provided. The "left" part of T_3 consisted of the three vertical counters closest to the beam.

These "kinematical" combinations of counters in the beam and behind the spark chamber telescopes were combined with the information from the Čerenkov counters in the incident beam. For target 1 events, only kaons or antiprotons were allowed as beam particles. For target 2 events, no restriction on the type of the incoming particle was imposed. However, an extra dead-time was imposed on pion-induced reactions to suppress the event rate of pions in target 2.

The event triggers were thus the following:

E_1: $T_1(\text{down}) \cdot T_3(\text{right, up}) \cdot \bar{\pi} \cdot \overline{T_4}$

E_2: $T_1(\text{up}) \cdot T_3(\text{right, down}) \cdot \bar{\pi} \cdot \overline{T_4}$

E_3: $T_1(\text{down}) \cdot T_3(\text{left, up}) \cdot \bar{\pi} \cdot \overline{T_4}$

E_4: $T_1(\text{up}) \cdot T_3(\text{left, down}) \cdot \bar{\pi} \cdot \overline{T_4}$

E_5: $T_1 \cdot T_3(\text{left, up}) \cdot K \cdot \check{C}W_3$

E_6: $T_1 \cdot T_3(\text{left, down}) \cdot K \cdot \check{C}W_3$

E_7: $T_4(\text{down}) \cdot T_3(\text{right, up}) \cdot \overline{T_1}$

E_8: $T_4(\text{up}) \cdot T_3(\text{right, down}) \cdot \overline{T_1}$

These event triggers initiated the following operations:

i) the high-voltage pulses on the spark chambers were switched on;
ii) the fast electronics were gated off for an imposed dead-time of 10 msec;
iii) the signals from all the trigger logic fired by an event were stored in CAMAC memory gates;
iv) after a delay of 0.5 msec the computer started to read out all information related to the event, and
v) the pulsed clearing fields were switched on for the spark chambers.

The event triggers E_5 and E_6 were used to accumulate events $Kp \to \pi\Sigma$.

---

*) The symbols have the following meaning: The dot indicates a coincidence (AND)-circuit, the plus indicates an OR-circuit, the bar indicates an antisignal.

2.6 On-line computer

A Varian 620/i computer was used to control the data acquisition, to store the data on magnetic tapes, and to check the performance of the set-up. In particular the efficiency of wire chambers, scintillation counters, and Čerenkov counters was examined regularly. The Varian had a ferrite core memory of 24K. Each word was 18 bits, of which only 16 were used. The quantities transmitted to the computer were the content of 16 binary scalers, the counter information, and the spark chamber data.

The binary scalers contained mainly the numbers of incident particles of each kind. Each scaler occupied one word. All the fired counters were registered, occupying one bit each. The spark chamber information was decoded[1] into binary addresses of clusters and sizes of the clusters.

At the end of each data file, the decimal scalers were read out. They contained the integral of all the different particles in this particular file. The binary scalers were reset after each event, but, as they were read each time, these two systems of scalers provided a control on the number of incident particles. Each event occupied at most 254 words. Typically 5 events were registered during each burst.

3. DATA ANALYSIS

The data from the main run was stored on 72 magnetic tapes, with roughly 50,000 triggers on each. Some of the tapes contained files with test data and were thus not included in the analysis.

The inelastic events were filtered out on the basis of cuts on kinematical variables alone, with no additional fitting procedure. The background of inelastic events in the data was sufficiently small so that this procedure imposed no problems in the estimate of the background.

Those triggers which fulfilled the criteria for elastic events were put on data summary tapes. A Monte Carlo program calculated the acceptance of the apparatus. The analysis was done at the CERN CDC 7600 computer.

In the following a brief description is given of how the geometrical reconstruction of the events was performed by the programs. This set of reconstruction programs was used to make final adjustment of the coordinate of the set up, and furthermore the kinematical parameters were also obtained. After a description of the acceptance calculation the effect of the background and other corrections upon the cross-section are discussed.

3.1 Geometrical reconstruction

3.1.1 Beam

The position and direction of the incoming particle were obtained from two sets of scintillation hodoscopes, about 8 m apart. In the beam were also mounted two proportional wire chambers. It was required to have one or two neighbouring hits in each scintillation hodoscope plane. If the information from the counters was missing, the corresponding information was obtained from the proportional chambers. In this way the beam-efficiency was improved from about 70% to about 85%.

3.1.2 Chambers

The horizontal and vertical projection in each of the telescopes W_2, W_3, and W_4 had all possible track-projections recorded, defined by three or four clusters on a straight line. The slope and position were obtained with the least-squares method*). A maximum of eight tracks were accepted in each projection. On the basis of the number of three- and four-cluster projections, the efficiency of the chambers could be calculated.

3.1.3 Vertex reconstruction

The distance between the beam track and each of the tracks in W_1 or W_4 was calculated. If this distance was less than 7 mm in target 1 and 11 mm in target 2, the telescope track was accepted. The midpoint between these two lines was defined as the vertex point. If more than one vertex point remained, after all the telescope tracks had been tried, the track with the shortest distance to the beam was used in the further analysis. When such an ambiguity occured, the main reason was a cluster split with more than one wire between the two parts of the cluster.

The tracks in W_3 were then extended to the midplane in the magnet, and the straight line between this point and the vertex defined the direction of the other outgoing track from the vertex. This method of reconstructing the scattering angle was tested on Monte Carlo generated events.

3.2 Alignments

The positions of the chambers within each telescope were adjusted by examining the distance from the clusters to the least squares fit line to a track, for a large number of tracks. The position and orientation of each telescope relative to the beam were obtained from a special run with low beam intensity and with no field in the magnet. These adjustments were based on geometry alone, with no requirements from kinematics being introduced. Likewise, the positions of the counters were adjusted. When afterwards compared with the kinematical parameters, the results were compatible with a beam momentum of 6,2 ± 0.1 GeV/c.

---

*) The counter in line with the projection of the track was required to be fired.

3.3 Kinematical tests

The directions of the incoming and the outgoing particles and the measured momentum of one of the outgoing particles were compared with the criteria for elastic events: the coplanarity, the scattering angle (θ) of the forward-going particle, and the momentum of the forward-going particle (p). These three parameters are not independent, but their influence varies differently through the t-range and they thus tend to complement each other. An elastic event must then satisfy all three criteria, within certain limits. We thus represent each event as a point in a three-dimensional (non-orthogonal) space. The excess of points around coplanarity, $\Delta\theta$ and Δp, all equal to zero, are the number of elastic events in the sample. The density of points in this space, outside this region, indicates the background.

3.3.1 Coplanarity test

The coplanarity was defined as the scalar three-vector product

$$R = (\hat{v}_{beam} \times \hat{v}_{wa}) \cdot \hat{v}_{wb} ,$$

where $\hat{v}_{beam}$ is the unit vector of the beam particle, $\hat{v}_{wa}$ is the unit vector of the track in W_1 or W_4, and $\hat{v}_{wb}$ is the unit vector from the vertex to the reconstructed point in the midplane of the magnet. The effect on R of the magnetic field is a second-order effect, and the distribution of R with test data, with the field in the magnet off, showed almost no difference from data with the magnet on.

During the DST production run the events were accepted if $|R| \leq 0.01$ for target 1 and $|R| \leq 0.02$ for target 2. In the final cross-section calculation the value $|R| \leq 0.01$ was used for all the events. The distribution of R from a set of events from target 1 is shown in Fig. 2.

3.3.2 Test of scattering angle

From the knowledge of the type of incoming particle and from the angle between the beam and the W_1-track (or W_4-track), the angle of the other scattered charged particle could be calculated, assuming elastic kinematics. The difference $\Delta\theta$ between this calculated value and the measured value was subject to a cut. We examined the $\Delta\theta$ distribution with and without the magnetic field, and no significant difference was observed. For target 1 the cut-off values in the DST production run was given by -0.015 rad $< \Delta\theta \leq 0.020$ rad for target 1, and -0.025 rad $\leq \Delta\theta \leq 0.030$ rad for target 2.

In the cross-section calculations the value was -0.012 rad $\leq \Delta\theta \leq 0.012$ rad for target 1, and -0.015 rad $< \Delta\theta < 0.015$ rad for target 2.

The distribution of $\Delta\theta$ for events from target 1 is shown in Fig. 2.

3.3.3 Momentum measurement and test

The main purpose of the magnet was to filter out background particles with low momentum, and to obtain the charge of the particle in an easy way.

The momentum was obtained from an inverse interpolation method given the vertex, the point in the middle of the magnet, and the deflection angle[13]. If the difference $|\Delta p|$ between the calculated momentum (obtained during the calculation of scattering angle, mentioned above) and the momentum obtained from the inverse interpolation method was greater than the cut-off value, the event was rejected. During production runs, the cut-off test was $|\Delta p| \leq 1.5$ GeV/c for target 1 and $|\Delta p| \leq 2.0$ GeV/c for target 2. In the cross-section calculation, $|\Delta p| \leq 0.7$ GeV/c for target 1 and $|\Delta p| \leq 0.8$ GeV/c for target 2.

The distribution of Δp for events from target 1 is shown in Fig. 2.

3.4 Acceptance calculations

The geometrical acceptance of the apparatus, as a function of t, was obtained by a Monte Carlo type calculation. The observed beam profile was used. Absorption in the targets and their surroundings, low momentum cut-off of protons in W_1, Coulomb scattering in target 1 (for target 2 events), and decay in flight of outgoing pions or kaons were included.

The results are shown in Fig. 3.

3.5 Cross-section calculation

The total number of events used in the cross-section calculation was 119,900 for target 1 and 1,200 for target 2. The cross-section for reactions in each of the two targets was calculated separately, using the acceptance values obtained for each target. In the final results several effects have been considered.

3.5.1 Cut-off values on kinematical parameters

Each event is represented by a point in a three-dimensional space with axes representing coplanarity, $\Delta\theta$ and Δp. From the density of points in this space in the neighbourhood of the cuts, it is possible to estimate how many elastic events are outside the cuts and also how much background is inside. We will discuss the different kinematical regions separately.

a) Forward angular region $[-t < 3.0\ (\text{GeV/c})^2]$

Two-dimensional scatter plots of any combination of variables $\Delta\theta$, Δp, and coplanarity, were studied, with data from a special test run. Owing to some extent to cluster split, 10 ± 2% of the elastic events are lost outside the cuts. These events have the same t-dependence as the other elastic events. The amount of inelastic events inside the cuts is 0.8 ± 0.2%.

b) Large angular region $[3.0\ (GeV/c)^2 < -t < 9.0\ (GeV/c)^2]$

An approach similar to that mentioned above was utilized when studying the data in the large angular region. With somewhat larger cuts for $\Delta\theta$ and Δp, within the accuracy given by statistics no elastic events were outside the cuts. The background of inelastic events inside the cuts was examined for the following t-bins [in $(GeV/c)^2$]: 3.0-3.2, 3.2-3.5, 3.5-4.0, and 4.0-9.0.

The background in the bin 3.0-3.2 $(GeV/c)^2$ was estimated to 10 ± 6%. The background in the three other bins was estimated to 24 ± 10%. In Figs. 4a and 4b are shown scatter plots of coplanarity versus $\Delta\theta$ for all events from target 2. Events with Δp outside the cut-off value are indicated by open circles. The events were randomly distributed in time, during the whole run. All events in the 90° c.m. scattering region were displayed, and were consistent with being genuine elastic events.

c) Backward angular region $[9.0\ (GeV/c)^2 < -t < 10.0\ (GeV/c)^2]$:

As above, we obtain information on the background inside the cut-off values from the scatter plot (Fig. 4c). All events giving a signal (π) in the Čerenkov counter behind W_3 have been removed. In this region, the background is definitely larger than in the other regions. Of the 17 ± 4 events inside the cuts, 7 ± 3 are background events. This gives a cross-section, after background subtraction, of 30 ± 15 nb/$(GeV/c)^2$.

3.5.2 δ-rays in the target

A separate Monte Carlo run was performed to study the effects of δ-rays being produced by the particles travelling in the targets, and hitting one of the anti-counters around the targets and thus quenching the event. We assume that the lower limit of the kinetic energy of the electron to be detected is 0.5 MeV. Within the statistical uncertainties we observe no t-dependence of this event loss. For target 1 the loss is estimated to be 17 ± 5%, and for target 2, 35 ± 8%. (For target 2, see Section 3.5.6.).

3.5.3 Random veto

A random veto of an event can occur when two particles are close in time and when one particle reacts in the target while the other hits the veto counter behind the target. With a resolution time of the veto counter equal to 25 nsec, the burst time 350 msec and 5×10^5 particles per burst, there will be an event vetoed 3.6 ± 0.9% of the time, assuming a random distribution of particles within the spill. The extra dead-time for the other anticounters was examined by comparing the cross-section for a test run at low beam intensity with the results from an ordinary run. The difference was 10 ± 3%.

3.5.4 Absorption in the incident beam

The material (scintillators, target window, and proportional chambers) in the beam line upstream of target 1 (Fig. 1) caused 6 ± 2% of the antiprotons to interact and pass through the hole of the V_1 counter.

The possibilities that an incident pion might interact upstream in front of the first Čerenkov counter, producing a proton in the forward direction, have been investigated. This could make a backward peak in the cross-section. Because of the small hole in V_1, less than 0.1% of the large-angle events would be affected in this way, all having wrong kinematics.

3.5.5 Program chain

An elastic event could be missed in the analysis for several reasons: too many tracks in a telescope, inconsistent counter information, a track missing in a telescope, etc. These effects were kept track of in the program chain and included directly in the cross-section calculation. One exception was a 3 ± 1% effect, mainly from missing momentum information for target 2.

3.5.6 Absorption effect of scattered particles

For target 1, the correction for reactions in spark chambers and in air was estimated to 9.5 ± 2.0% for forward scattering and 6.9 ± 2.0% for backward scattering. For target 2 the correction was 7.0 ± 2.0%.

3.5.7 The overlap region of t for target 1 and target 2

The data from target 1 and target 2 had an overlap region of 1.55 $(GeV/c)^2 < -t < 2.75$ $(GeV/c)^2$, consisting of 11 bins. Applying only the acception corrections (3.4), the cross-section values for target 2 were all lower than the corresponding cross-section values for target 1. A weighted average for all the bins was calculated, and one obtained a ratio equal to 1.38 ± 0.05 for the two samples of data.

3.5.8 Summary

The effects mentioned above, and not included in the Monte Carlo calculation, made up a normalization factor for the cross-section calculation. In the forward direction this factor was 1.8 ± 0.2. In the large angular region the factor was 2.2 ± 0.3. This higher value was consistent with what was observed in the overlap region (Section 3.5.7). The factor obtained for the backward region was 1.8 ± 0.2.

In the cross-section calculation the observed value (Section 3.5.7) was used to normalize the large-angle data to the rest of the data. A factor of 1.8 was then used as an over-all normalization factor.

The observed background in the large angular and backward regions was subtracted, and the corresponding uncertainty folded in in the cross-section calculations.

Furthermore, correction for beam efficiency and angular spark chamber efficiencies were included, taking into account possible changes during the run.

The calculated beam and spark chamber efficiencies had an estimated error of 5% and 10%, respectively. The uncertainty in acceptance calculations is estimated to be 5%. These uncertainties added to the uncertainty in the normalization implies an over-all uncertainty of 20% in the absolute normalization.

4. RESULTS

The cross-sections, based on the number of observed events, acceptance calculations, and normalization factors are given in Table 1.

The errors are statistical errors only, based on number of observed events, possible background subtraction and Monte Carlo calculation, the last one being much smaller than the other two.

The results are plotted in Fig. 5, together with our earlier 5 GeV/c results. In Fig. 6 the angular distributions of the same data are displayed. The dip region around $-t = 0.5$ is displayed in Fig. 7. There are some indications that the following maximum around $-t = 0.7$ $(GeV/c)^2$ is decreasing with energy. A shoulder at about $t = -2.2$ $(GeV/c)^2$, first observed at 5 GeV/c [1], is also present in these data (Fig. 5). The data in this forward direction have been analysed elsewhere[15], based on an impact parameter picture[16]. Fitting the data up to $-t = 3$ $(GeV/c)^2$, one obtains 0.8 fermi as interaction radius.

In the large angular region, around the 90° c.m. scattering angle, the 6.2 GeV/c data again follow the same general pattern as the 5 GeV/c data. An s-dependence of s^{-10} would imply a ratio of 6.0 between the two sets of data for the 90° c.m. scattering angle region. Our data indicate a lower s-dependence value in this region.

We observe from Figs. 5 and 6 that the cross-section in the backward region is decreasing by an order of magnitude between 5 and 6.2 GeV/c.

Table 1

Differential cross-section for $\bar{p}p$ elastic scattering at 6.2 GeV/c; $s = 13.528\ (GeV)^2$, $E_{cm} = 6.678$ GeV

$-t$ $(GeV/c)^2$	Δt	$d\sigma/dt$ $\mu b/(GeV/c)^2$	Error
0.31	0.02	2377	64
0.33	"	1771	49
0.35	"	1253	36
0.37	"	918	16
0.39	"	647	12
0.41	"	466	11
0.43	"	342	10
0.45	"	261	8
0.47	"	193	7
0.49	"	160	6
0.51	"	147	6
0.53	"	132	5
0.55	"	134	5
0.57	"	136	5
0.59	"	141	5
0.61	"	145	5
0.63	"	159	6
0.65	"	169	6
0.67	"	177	7
0.69	"	183	7
0.71	"	167	6
0.73	"	184	7
0.75	"	181	7
0.77	"	172	7
0.79	"	166	6
0.81	"	176	7
0.83	"	165	7
0.85	"	170	7
0.87	"	151	6
0.89	"	150	6
0.91	"	153	7
0.93	"	136	6
0.95	"	133	6

Table 1 (cont.)

$-t$ $(GeV/c)^2$	Δt	$d\sigma/dt$ $\mu b/(GeV/c)^2$	Error
0.97	"	115	6
0.99	"	123	6
1.02	0.04	112	4
1.06	"	100	4
1.10	"	83.4	2.8
1.14	"	68.4	2.8
1.18	"	60.6	2.7
1.22	"	50.8	2.5
1.26	"	44.6	2.4
1.30	"	41.4	2.2
1.34	"	29.8	1.9
1.38	"	24.9	1.7
1.42	"	21.1	1.6
1.46	"	18.7	1.5
1.49	0.02	15.7	2.0
1.55	0.1	12.0	0.73
1.65	"	10.4	0.70
1.75	"	7.94	0.60
1.85	"	7.70	0.60
1.95	"	5.47	0.48
2.05	"	5.15	0.43
2.15	"	5.32	0.47
2.25	"	5.16	0.47
2.35	"	4.60	0.46
2.45	"	3.78	0.42
2.55	"	3.28	0.42
2.65	"	2.68	0.40
2.75	"	2.59	0.40
2.85	"	1.69	0.40
2.95	"	1.44	0.34
3.05	"	1.04	0.33
3.15	"	0.93	0.35
3.35	0.3	0.33	0.15
4.00	1.0	0.077	0.046
5.50	2.0	0.026	0.021
7.75	2.5	0.0074	0.0059
9.5	1.0	0.030	0.015

REFERENCES

1) A. Eide, P. Lehmann, A. Lundby, C. Baglin, P. Briandet, P. Fleury, P.J. Carlson, E. Johansson, M. Davier, V. Gracco, R. Morand and D. Treille, Nuclear Phys. B60 (1973) 173.

2) C. Baglin, P. Briandet, P.J. Carlson, B. d'Almagne, A. Eide, P. Fleury, V. Gracco, E. Johansson, P. Lehmann, A. Lundby, S. Mukhin, A. Navarro-Savoy, A. Pevsner, F. Richard, G. de Rosny, L. Staurset and D. Treille, Phys. Letters 47B (1973) 85.

3) C. Baglin, P. Briandet, P.J. Carlson, B. d'Almagne, A. Eide, P. Fleury, V. Gracco, K.E. Johansson, P. Lehmann, A. Lundby, A. Navarro-Savoy, F. Richard, G. de Rosny, L. Staurset, and D. Treille, Elastic scattering of 10 GeV/c protons on protons (to be published).

4) C. Baglin, P. Briandet, P.J. Carlson, B. d'Almagne, A. Eide, P. Fleury, V. Gracco, E. Johansson, P. Lehmann, A. Lundby, S. Mukhin, A. Navarro-Savoy, A. Pevsner, F. Richard, G. de Rosny, L. Staurset and D. Treille, Phys. Letters 47B (1973) 89.

5) B. Barish, D. Fong, R. Gomez, D. Hartill, J. Pine, A.V. Tollestrup, A. Maschke, and T.F. Zipf, Phys. Rev. Letters 17 (1966) 720.

6) D.L. Parker, B.Y. Oh, G.A. Smith and R.J. Sprafka, Nuclear Phys. B32 (1971) 29.

7) V. Domingo, G.P. Fisher, L. Marshall Libby and R. Sears, Phys. Letters 24B (1967) 642.

8) B. Escoubès, A. Fedrighini, Y. Goldschmidt-Clermont, M. Guinea-Moorhead, T. Hofmokl, R. Lewish, D.R.O. Morrison, M. Schneeberger and S. de Unamuno, Phys. Letters 5 (1963) 132.

9) W.M. Katz, B. Forman and T. Ferbel, Phys. Rev. Letters 19 (1967) 265.

10) D. Birnbaum, R.M. Edelstein, N.C. Hien, T.J. McMahon, J.F. Mucci, J.S. Russ, E.W. Anderson, E.J. Bleser, H.R. Blieden, G.B. Collins, D. Garelick, J. Menes and F. Turkot, Phys. Rev. Letters 23 (1969) 663.

11) Yu.M. Antipov, G. Ascoli, R. Busnello, G. Damgaard, M.N. Kienzle-Focacci, W. Kienzle, R. Klanner, L.G. Landsberg, A.A. Lebedev, C. Lechanoine, P. Lecomte, M. Martin, V. Roinishvili, R.D. Sard, A. Weitsch and F.A. Yotch.

12) D. Meyer, 17th Internat. Conf. on High-Energy Physics, London 1974, I-29.

13) C. Lechanoine, M. Martin and H. Wind, Nuclear Instrum. Methods 69 (1969) 122.

14) E. Johansson, Hadron-hadron elastic scattering and annihilation reactions at 5 and 10 GeV/c, thesis, University of Stockholm, 1974.

15) P. Helgaker, Antiproton-proton elastic scattering at 6.2 GeV, thesis, University of Oslo, 1975.

16) H.I. Miettinen, CERN TH. 1864.

Figure captions

Fig. 1 : Experimental layout.

Fig. 2 : The distribution of kinematical parameters, coplanarity, Δp and $\Delta\theta$.

Fig. 3 : The acceptance as a function of $-t$ for $\bar{p}p$ elastic scattering for events in target 1 and in target 2.

Fig. 4 : Scatterplot of coplanarity versus scattering angle, $\Delta\theta$, for different t-regions. The outside boundaries on the plots represent the limits used during production runs, whereas the inner boundaries were used when calculating the cross-sections. Open circles represent events with Δp outside the limits used during cross-section calculation. All events with a signal (π) in the Čerenkov counter behind W_3 have been removed on Fig. 4c.

Fig. 5 : The differential cross-section for $\bar{p}p$ elastic scattering as a function of $-t$, for this experiment and our earlier experiment at 5 GeV/c (Ref. 1).

Fig. 6 : The differential cross-section for $\bar{p}p$ elastic scattering as a function of $\cos\theta_{cm}$, for this experiment and our earlier experiment at 5 GeV/c (Ref. 1).

Fig. 7 : The differential cross-section for $\bar{p}p$ forward elastic scattering as a function of $-t$. The data at 3.66 GeV/c is from Katz et al. (Ref. 9), at 5.0 GeV/c from Eide et al. (Ref. 1), at 6.2 GeV/c from this experiment, and at 8.0 GeV/c and 16.0 GeV/c from Birnbaum et al. (Ref. 10).

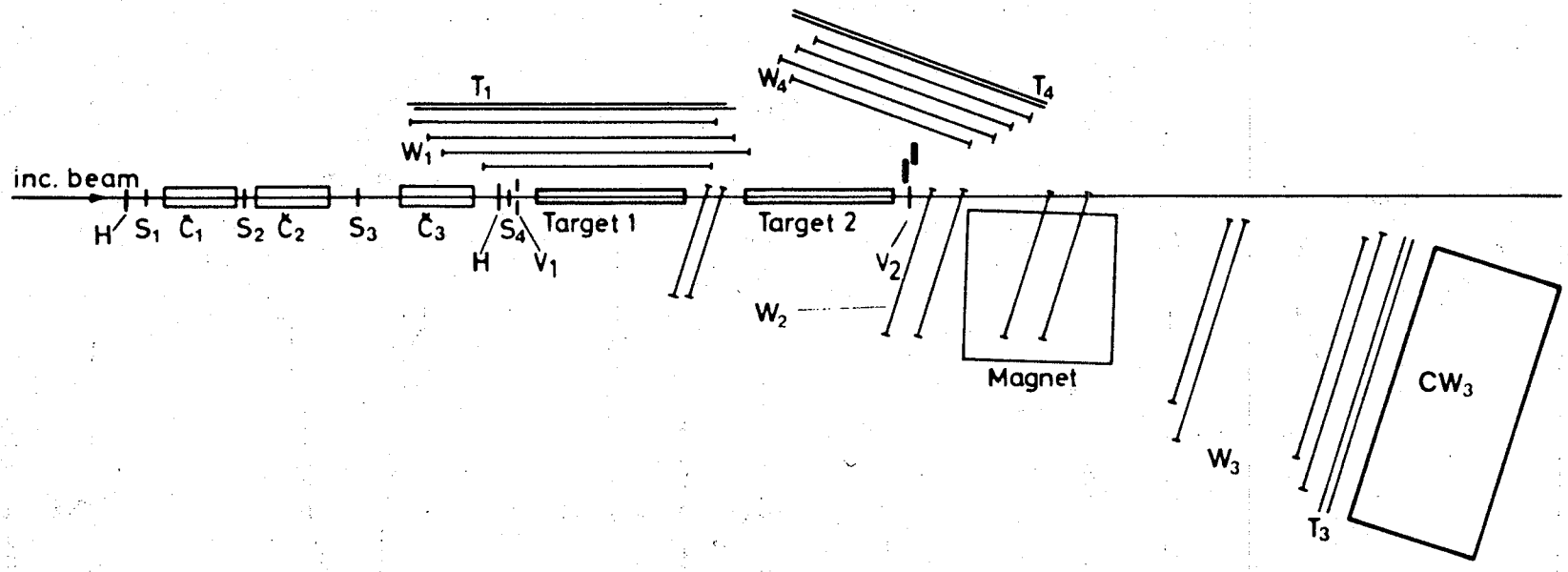
T1
W4
T4
W1
inc. beam
H
S1
Č1
S2
Č2
S3
Č3
H
S4
V1
Target 1
Target 2
V2
W2
Magnet
W3
CW3
T3

Fig. 1

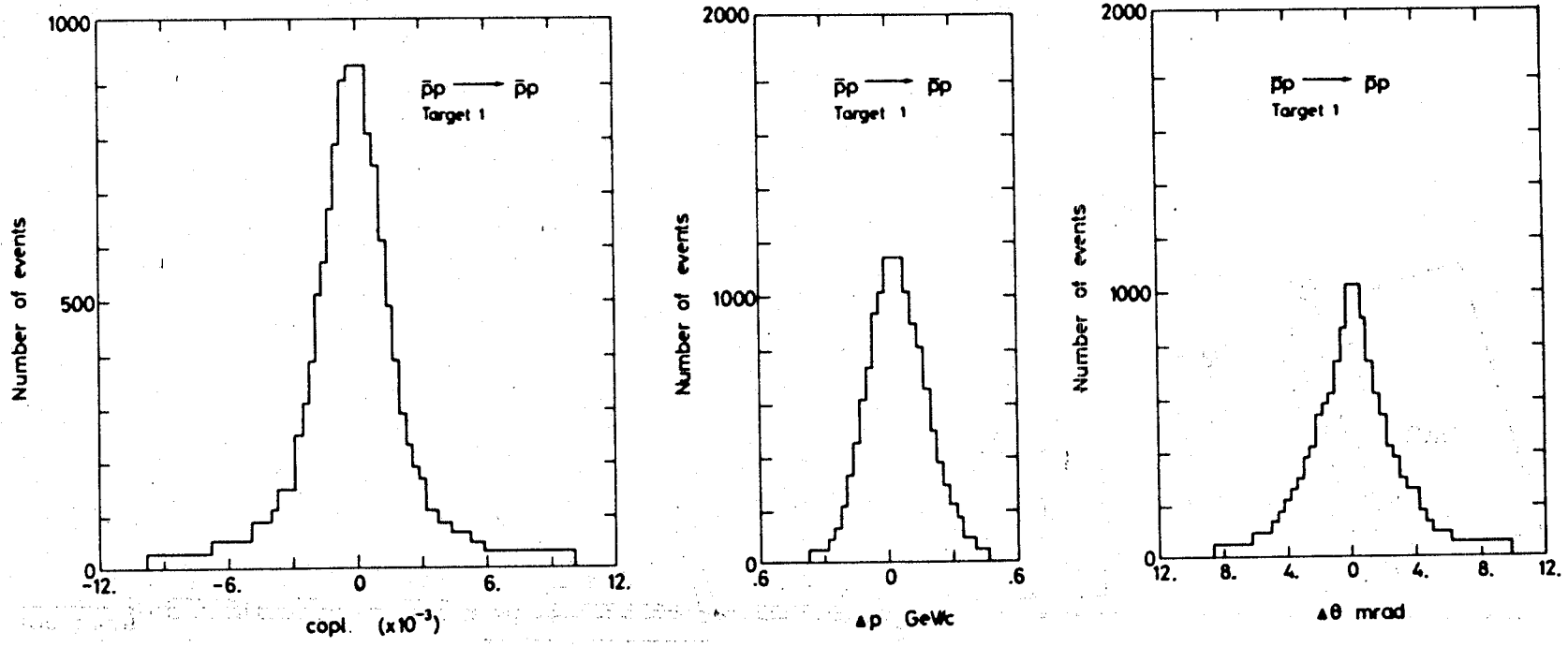
1000
500
0
Number of events
$\bar{p}p \longrightarrow \bar{p}p$
Target 1
-12.
-6.
0
6.
12.
copl. ($\times 10^{-3}$)
2000
1000
0
Number of events
$\bar{p}p \longrightarrow \bar{p}p$
Target 1
.6
0
.6
Δp GeV/c
2000
1000
0
Number of events
$\bar{p}p \longrightarrow \bar{p}p$
Target 1
12.
8.
4.
0
4.
8.
12.
$\Delta\theta$ mrad

Fig. 2

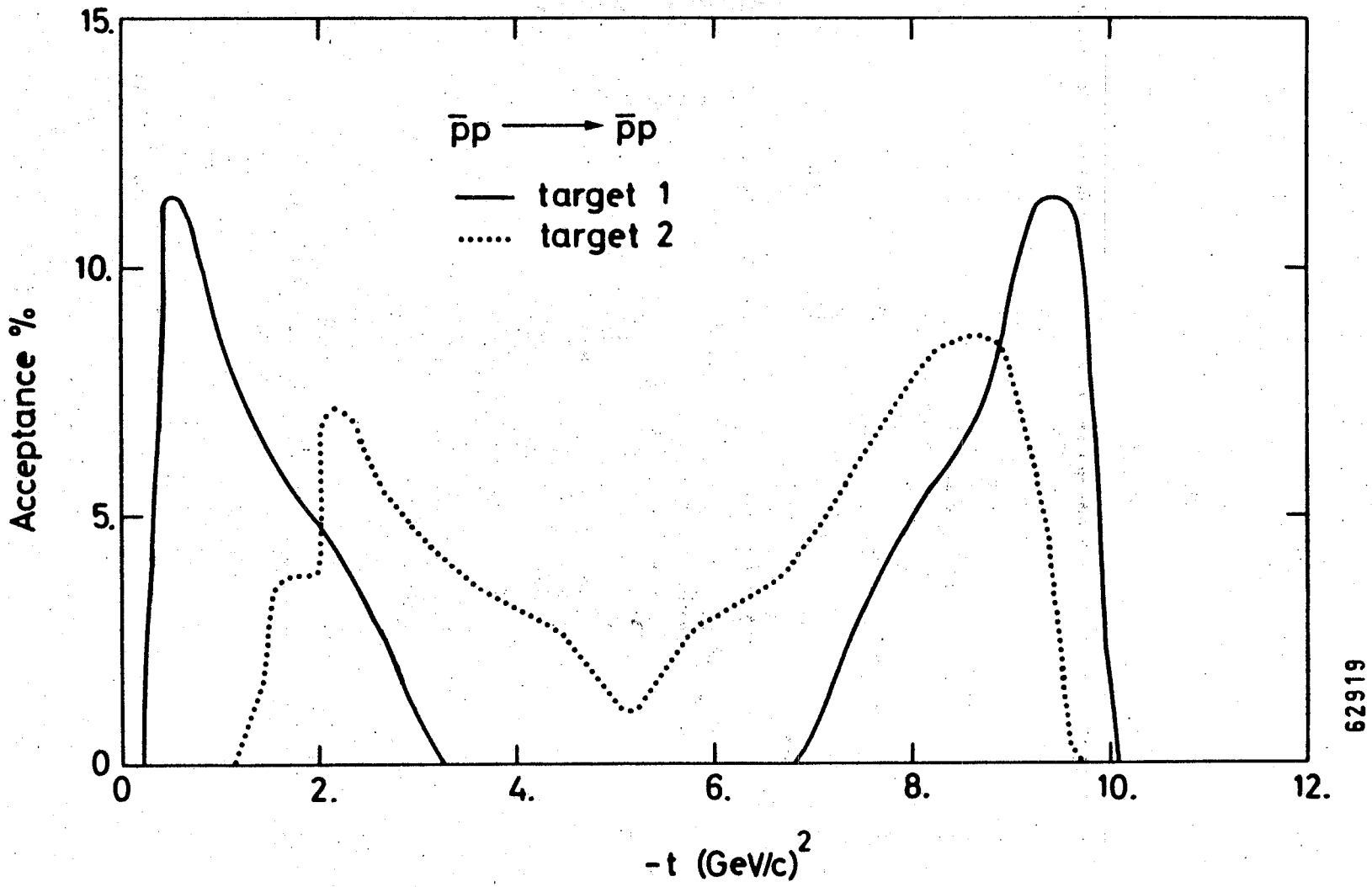
15.
10.
5.
0
0
2.
4.
6.
8.
10.
12.
Acceptance %
$\bar{p}p \longrightarrow \bar{p}p$
target 1
target 2
$-t\ (GeV/c)^2$
62919

Fig. 3

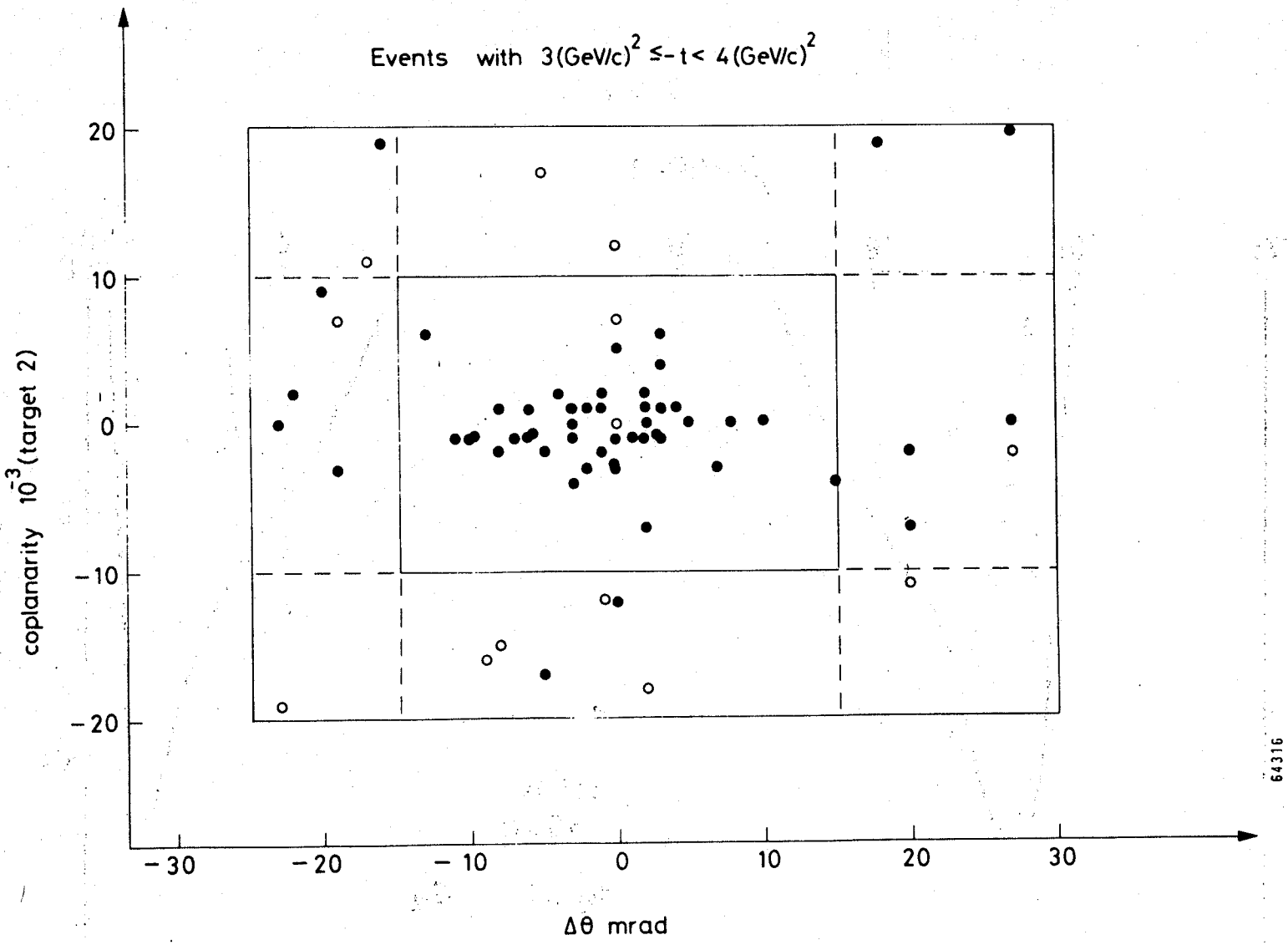
Events with 3(GeV/c)^2 ≤ -t < 4(GeV/c)^2
20
10
0
-10
-20
coplanarity 10^{-3}(target 2)
-30
-20
-10
0
10
20
30
Δθ mrad
64316

Fig. 4a

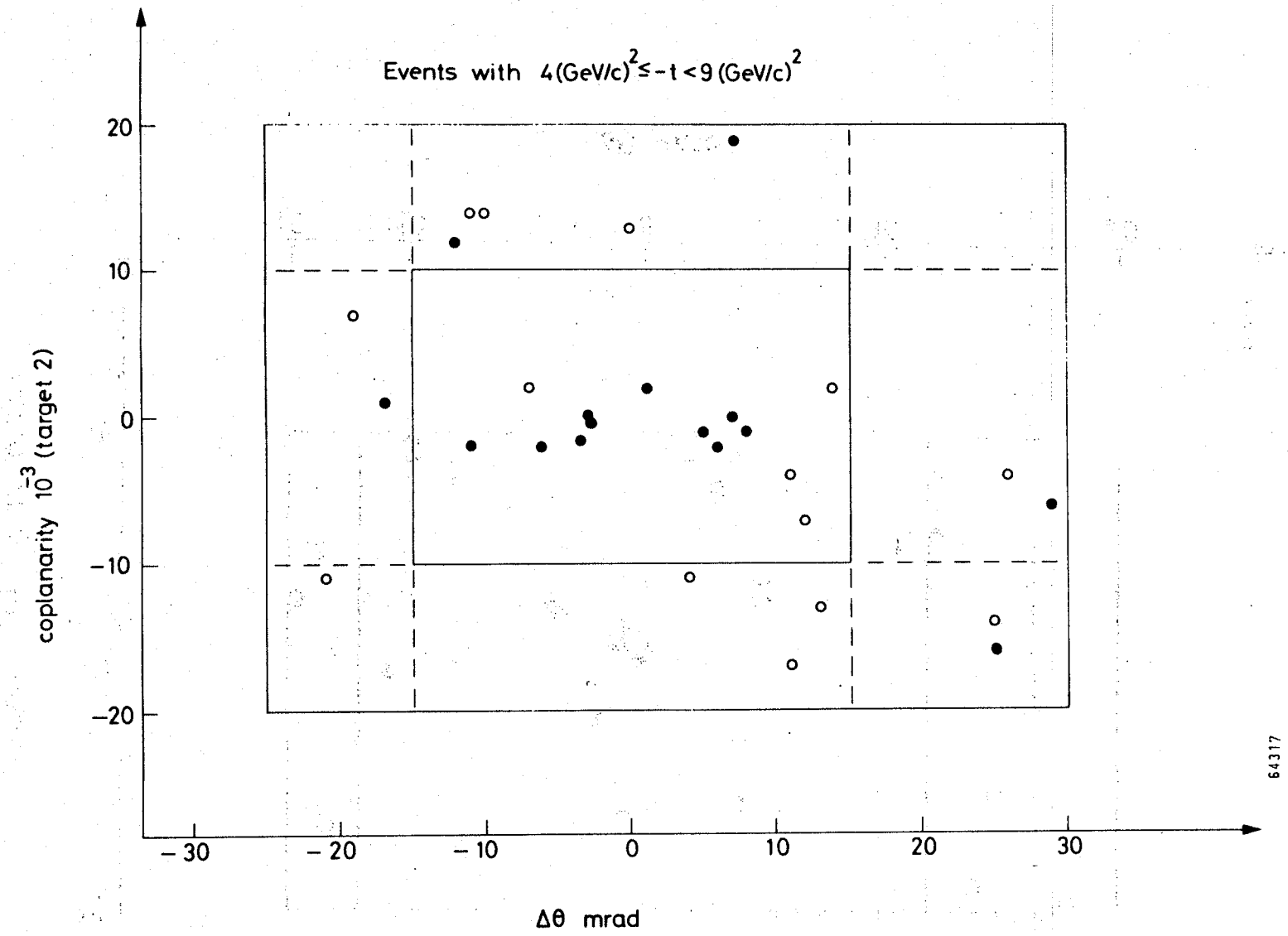
Events with $4(GeV/c)^2 \leq -t < 9(GeV/c)^2$
coplanarity 10^{-3} (target 2)
20
10
0
−10
−20
−30
−20
−10
0
10
20
30
Δθ mrad
64317

Fig. 4b

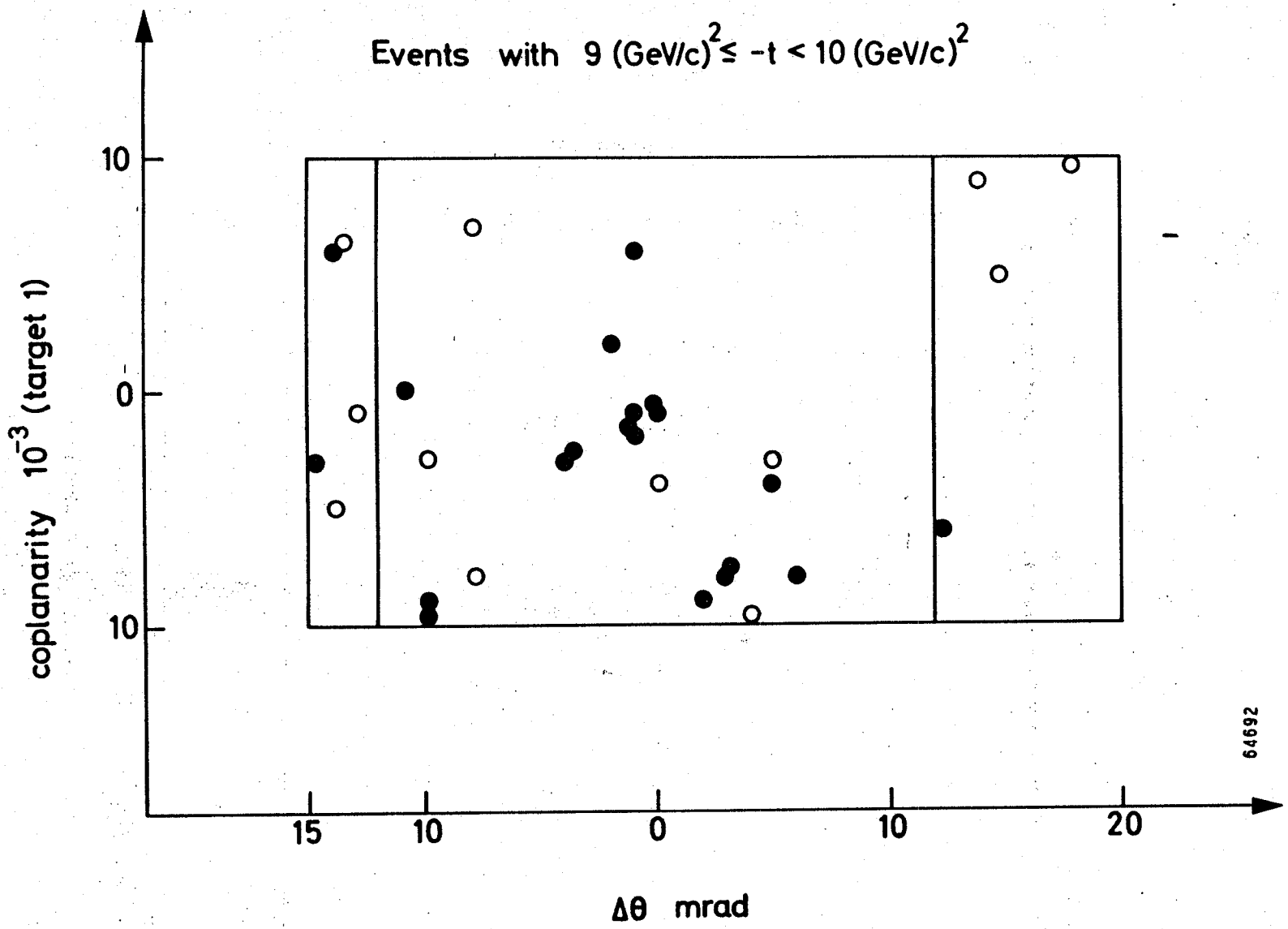
Events with 9 (GeV/c)^2 ≤ -t < 10 (GeV/c)^2
coplanarity 10^{-3} (target 1)
10
0
10
15
10
0
10
20
Δθ mrad
64692

Fig. 4c

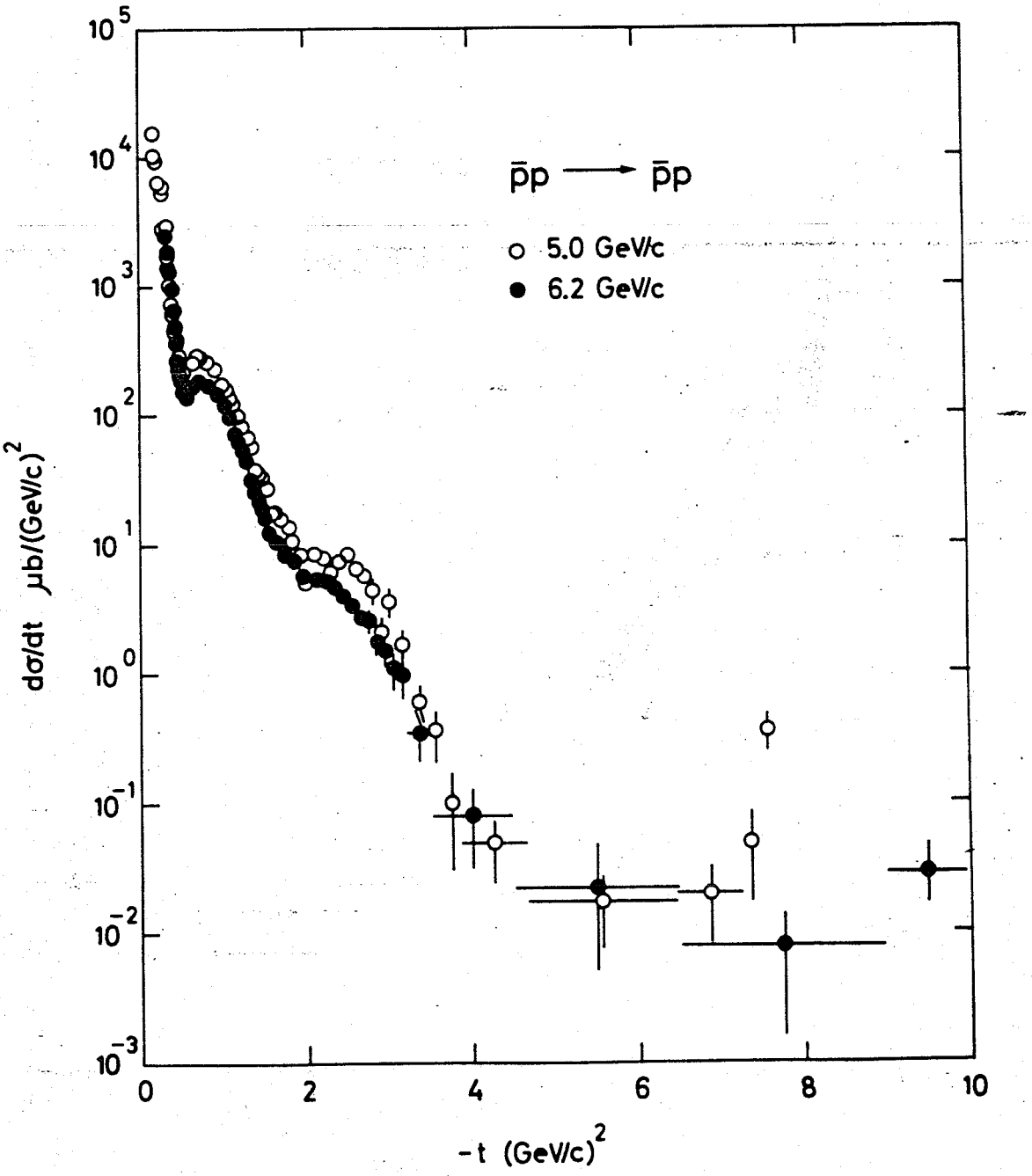
$\bar{p}p \longrightarrow \bar{p}p$
5.0 GeV/c
6.2 GeV/c
$d\sigma/dt$ $\mu b/(GeV/c)^2$
$-t$ $(GeV/c)^2$
10^5
10^4
10^3
10^2
10^1
10^0
10^{-1}
10^{-2}
10^{-3}
0
2
4
6
8
10

Fig. 5

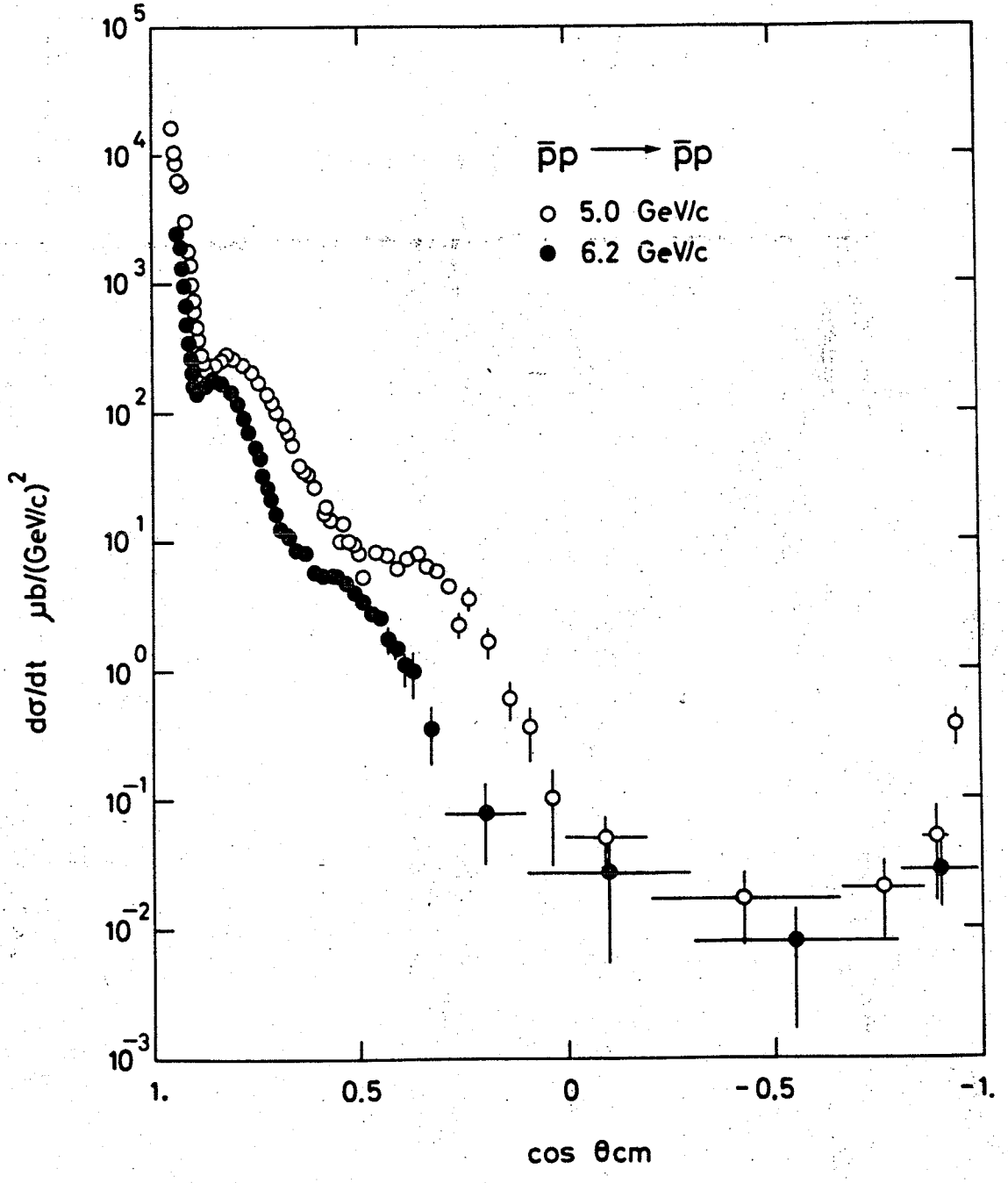
$\bar{p}p \longrightarrow \bar{p}p$
5.0 GeV/c
6.2 GeV/c
$d\sigma/dt$ $\mu b/(GeV/c)^2$
10^5
10^4
10^3
10^2
10^1
10^0
10^{-1}
10^{-2}
10^{-3}
1.
0.5
0
-0.5
-1.
cos θcm

Fig. 6

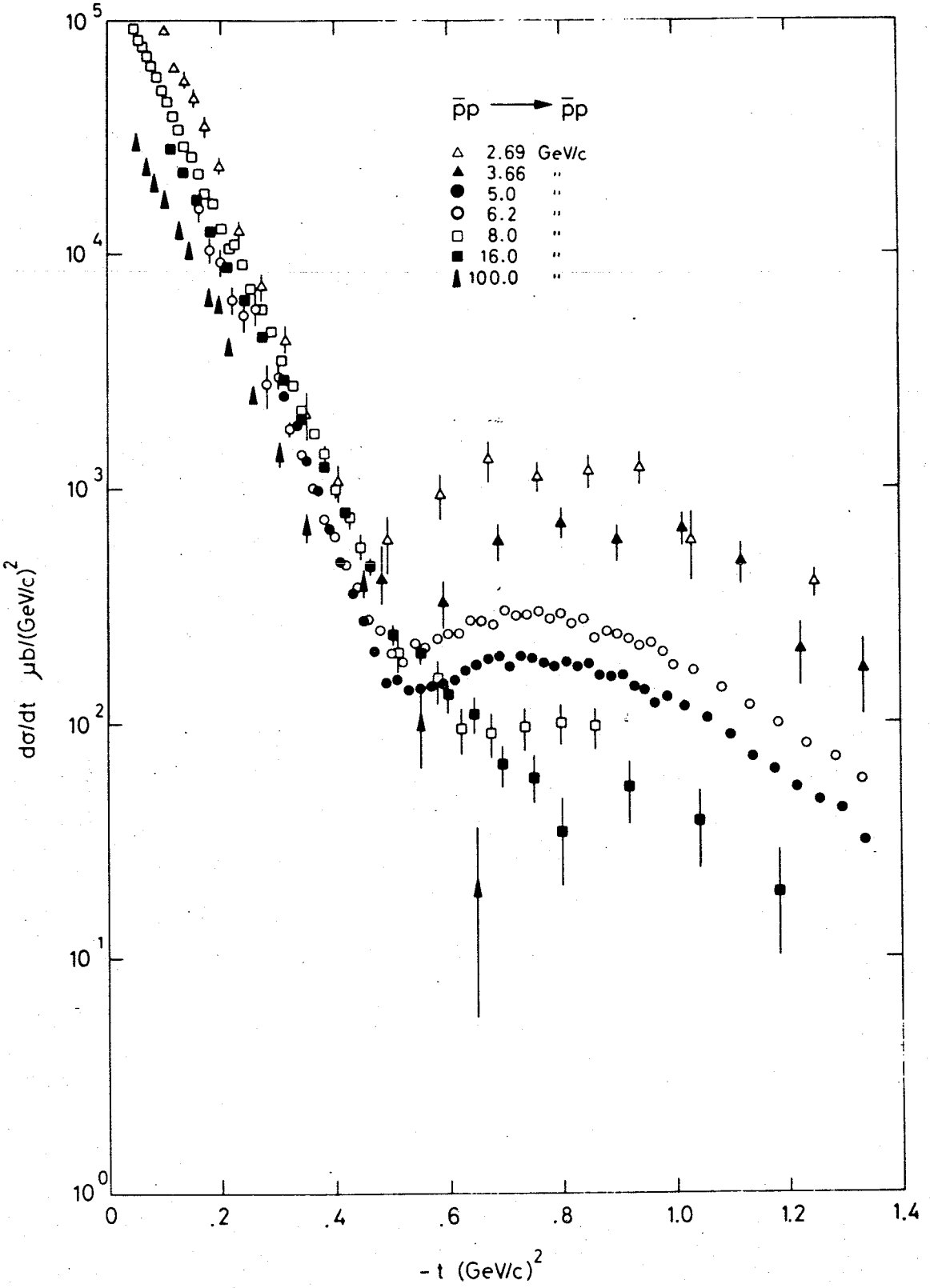
$\bar{p}p \longrightarrow \bar{p}p$
2.69 GeV/c
3.66 "
5.0 "
6.2 "
8.0 "
16.0 "
100.0 "
10^5
10^4
10^3
10^2
10^1
10^0
$d\sigma/dt$ $\mu b/(GeV/c)^2$
0
.2
.4
.6
.8
1.0
1.2
1.4
$-t$ $(GeV/c)^2$

Fig. 7